Imaging the Renner–Teller effect using laser-induced electron diffraction

Kasra Amini[a,b,1], Michele Sclafani[a,1], Tobias Steinle[a,1], Anh-Thu Le[c,2], Aurelien Sanchez[a], Carolin Müller[d], Johannes Steinmetzer[d], Lun Yue[d], José Ramón Martínez Saavedra[a], Michaël Hemmer[a], Maciej Lewenstein[a,e], Robert Moshammer[f], Thomas Pfeifer[f], Michael G. Pullen[a], Joachim Ullrich[f,g], Benjamin Wolter[a], Robert Moszynski[b], F. Javier García de Abajo[a,e], C. D. Lin[c], Stefanie Gräfe[d,h], and Jens Biegert[a,e,3]

[a]ICFO–Institut de Ciencies Fotoniques, The Barcelona Institute of Science and Technology, 08860 Castelldefels (Barcelona), Spain; [b]Department of Chemistry, University of Warsaw, 02-093 Warsaw, Poland; [c]Department of Physics, J. R. Macdonald Laboratory, Kansas State University, Manhattan, KS 66506-2604; [d]Institute of Physical Chemistry, Friedrich-Schiller University, 07743 Jena, Germany; [e]ICREA, 08010 Barcelona, Spain; [f]Max-Planck-Institut für Kernphysik, 69117 Heidelberg, Germany; [g]Physikalisch-Technische Bundesanstalt, D-38116 Braunschweig, Germany; and [h]Abbe Center of Photonics, Friedrich-Schiller University, 07745 Jena, Germany

Edited by Shaul Mukamel, University of California, Irvine, CA, and approved March 8, 2019 (received for review October 10, 2018)

Structural information on electronically excited neutral molecules can be indirectly retrieved, largely through pump–probe and rotational spectroscopy measurements with the aid of calculations. Here, we demonstrate the direct structural retrieval of neutral carbonyl disulfide (CS_2) in the $\tilde{B}^1B_2$ excited electronic state using laser-induced electron diffraction (LIED). We unambiguously identify the ultrafast symmetric stretching and bending of the field-dressed neutral CS_2 molecule with combined picometer and attosecond resolution using intrapulse pump–probe excitation and measurement. We invoke the Renner–Teller effect to populate the $\tilde{B}^1B_2$ excited state in neutral CS_2, leading to bending and stretching of the molecule. Our results demonstrate the sensitivity of LIED in retrieving the geometric structure of CS_2, which is known to appear as a two-center scatterer.

structural dynamics | electron diffraction | attosecond wave packet | laser-induced electron diffraction | nonadiabatic dynamics

Many important phenomena in biology, chemistry, and physics can be described only beyond the Born–Oppenheimer (BO) approximation, giving rise to nonadiabatic dynamics and the coupling of nuclear (vibrational and rotational) and electronic motion in molecules (1–7). One prominent example where the BO approximation breaks down is the Renner–Teller effect (8, 9): In any highly symmetric linear molecule with symmetry-induced degeneracy of electronic states, nonadiabatic coupling of (vibrational) nuclear and electronic degrees of freedom can lead to the distortion of the nuclear framework on a timescale comparable with electronic motion. The system's symmetry is then reduced by the bending of the molecule to split the degenerate electronic state into two distinct potential energy surfaces (PESs), leading to a more stable, bent conformer.

Here, we demonstrate the direct imaging of Renner–Teller nonadiabatic vibronic dynamics in neutral carbonyl disulfide (CS_2) with combined picometer and attosecond resolution through intrapulse pump–probe excitation and measurement with laser-induced electron diffraction (LIED) (10–16). Our results shed light on the vibronic excitation of a neutral linear molecule in the rising edge of our laser field that causes bending and stretching of the molecule. High-momentum transfers experienced by the electron wave packet (EWP) ($U_p = 85$ eV) with large scattering angles enable the electron to penetrate deep into the atomic cores, allowing us to resolve a strongly symmetrically stretched and bent CS_2 molecule most likely in the $\tilde{B}^1B_2$ excited electronic state.

Specifically, we pump and probe CS_2 molecules in a one-pulse LIED measurement to capture a single high-resolution snapshot of the molecular structure at around the peak of the strong laser field. By analyzing the angular dependence of the experimentally detected molecular interference signal, we directly retrieve a symmetrically stretched and bent CS_2^+ structure. We subsequently present results from state-of-the-art quantum dynamical calculations to investigate the mechanism behind the linear-to-bent transition that occurs in field-dressed CS_2.

Molecular Structure Extraction

Fig. 1 displays the results for three different electron returning energies, $E_R = 160$ eV, 170 eV, and 180 eV. From the measured momentum distribution, shown in Fig. 1*A*, the molecular differential cross-section (DCS) weighted by the molecular ionization rate and the alignment distribution is extracted using the quantitative rescattering (QRS) theory (*SI Appendix*). Molecular structural information is then obtained from the field-free molecular DCS via the molecular contrast factor (MCF). Fig. 1*B* shows the experimental MCF (black circles) and the theoretical MCFs corresponding to the equilibrium geometric structure of the $\tilde{X}^1\Sigma_g^+$ electronic ground state (orange trace) (9), the quasi-linear geometry (green trace) (17, 18), and the geometric structure that theoretically agrees best with the experimentally measured structure (red trace). Overall, there is a good fit

Significance

Laser-induced electron diffraction is a molecular-scale electron microscopy that captures clean snapshots of a molecule's geometry with subatomic picometer and attosecond spatiotemporal resolution. We induce and unambiguously identify the stretching and bending of a linear triatomic molecule following the excitation of the molecule to an excited electronic state with a bent and stretched geometry. We show that we can directly retrieve the structure of electronically excited molecules that is otherwise possible through indirect retrieval methods such as pump–probe and rotational spectroscopy measurements.

Author contributions: J.B. designed research; K.A., M.S., T.S., A.-T.L., A.S., C.M., J.S., L.Y., J.R.M.S., M.H., M.L., R. Moshammer, M.G.P., J.U., B.W., and J.B. performed research; A.-T.L., C.M., J.S., L.Y., J.R.M.S., R. Moszynski, F.J.G.d.A., C.D.L., and S.G. contributed new reagents/analytic tools; K.A., M.S., T.S., A.S., and M.G.P. analyzed data; and K.A., M.S., T.S., A.-T.L., M.L., R. Moshammer, T.P., J.U., R. Moszynski, F.J.G.d.A., C.D.L., S.G., and J.B. wrote the paper.

The authors declare no conflict of interest.

This article is a PNAS Direct Submission.

[1]K.A., M.S., and T.S. contributed equally to this work.

[2]Present address: Department of Physics, Missouri University of Science and Technology, Rolla, MO 65409.

[3]To whom correspondence should be addressed. Email: jens.biegert@icfo.eu.

This article contains supporting information online at www.pnas.org/lookup/suppl/doi:10.1073/pnas.1817465116/-/DCSupplemental.

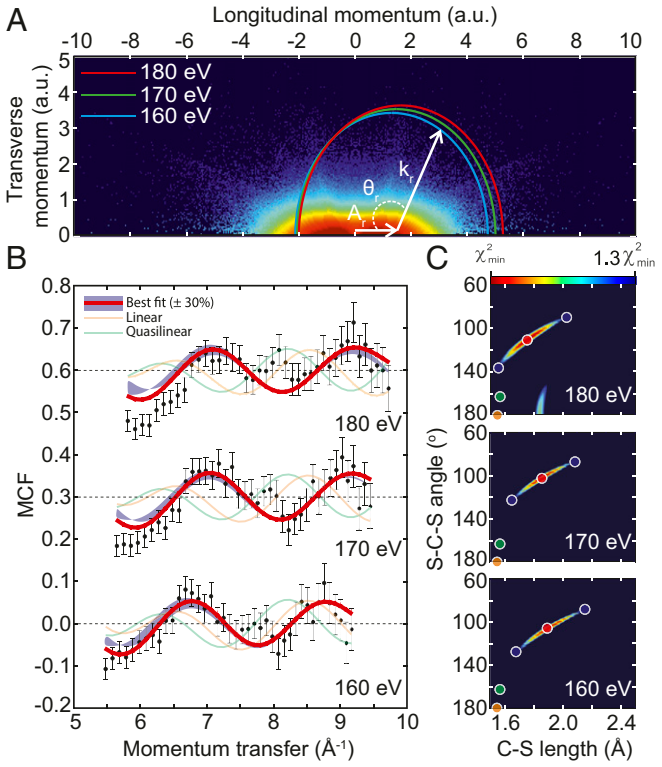

Fig. 1. LIED imaging of laser-induced skeletal deformations in CS_2. (*A*) Double differential cross-sections are extracted by integrating the experimental momentum distribution map along the rescattering angle, θ_r, of the circle defined by the parametric relations $p_{long} = -A_r \pm (k_r \times \cos\theta_r)$ and $p_{trans} = k_r \times \sin\theta_r$, where A_r is the value of the field vector at the time of rescattering. (*B*) Comparison of the experimental (black circles) molecular contrast factor (MCF) to the theoretical MCFs associated with the equilibrium geometric structure of the $\tilde{X}^1\Sigma_g^+$ electronic ground state (orange trace) (9), the quasilinear geometry (green trace) (17, 18), and the geometric structure that theoretically agrees best with the experimentally measured structure (red trace). The blue shaded region illustrates the sensitivity of the theoretical MCFs when varying R_{CS} and Φ_{SCS} by around ±0.25 Å and ±20°, respectively, corresponding to a 30% increase from the χ^2 minimum (*SI Appendix*). The data shown correspond to rescattered electrons with kinetic energies of 160 eV, 170 eV, and 180 eV. (*C*) CS_2 structural parameters are retrieved by locating the minimum of the χ^2 map (*SI Appendix*, Eq. **S1**). Here, the most probable CS_2 geometry (red circle in each plot) is shown along with a 30% variation of the χ^2 minimum (blue circles). The orange circle indicates the equilibrium geometry of neutral CS_2 in its $\tilde{X}^1\Sigma_g^+$ ground electronic state (1.55 Å, 180°) (9), whereas the green circle corresponds to CS_2 in a quasilinear configuration (1.54 Å, 163°) (17, 18).

between the experimental MCF and the theoretical MCF that best fits the experimental data. An additional peak is observed in the experimental data between 7.5 $Å^{-1}$ and 8.0 $Å^{-1}$ in Fig. 1*B* that is not captured by our best-fit single-structure theoretical MCF and is most likely due to a small contribution from another structure. Nevertheless, the single-structure fitting algorithm used in this work already agrees well with the experimental MCFs for a rather broad range of momentum transfer from around 5.5 $Å^{-1}$ to 9.5 $Å^{-1}$, and thus we believe that the extracted bent structure is the dominant one. Retrieving this information at different returning electron kinetic energies yields consistent results with bent and symmetrically stretched neutral CS_2, as shown in Fig. 1*C*.

Bent and Stretched Molecular Structure

The geometric parameters are retrieved from our LIED measurements as a function of the electron returning energy, as shown in Fig. 2. We measure a C-S bond length R_{CS} = 1.86 ± 0.23 Å and an S-C-S angle Φ_{SCS} = 104.0° ± 20.2°, which correspond to a strongly symmetrically stretched and bent molecule. Since field-free neutral CS_2 in the ground electronic state, $\tilde{X}^1\Sigma_g^+$, is linear in geometry (R_{eq} = 1.55 Å and Φ_{SCS} = 180°) (18), a linear-to-bent transition occurs that leads to the experimentally measured bent LIED structure.

Quantum Chemistry Dynamical Calculations

We performed advanced, state-of-the-art quantum dynamical calculations of coupled electron–nuclear motions on the field-dressed PESs in the presence of an intense laser field to investigate the mechanism behind such a linear-to-bent transition (*SI Appendix*). Our calculations reveal a Renner–Teller excitation mechanism that leads to the stretching and bending of neutral CS_2, with a schematic of the excitation shown in Fig. 3*A*. Optical excitation to the lowest-lying singlet excited electronic states, such as the doubly degenerate $^1\Delta_u$ state, from the $\tilde{X}^1\Sigma_g^+$ ground state in field-free neutral CS_2 is strictly dipole forbidden in the linear geometry ($D_{\infty h}$) due to symmetry considerations (gray arrow in Fig. 3*A*). However, in the presence of a strong field, our wave packet calculations in Fig. 4*A* show that the field-dressed (FD) molecule initially bends by ∼10° within 90 fs (blue rectangle in Fig. 4*A*) to split the degeneracy of $^1\Delta_u$ into two bent states ($\tilde{A}^1A_2$ and $\tilde{B}^1B_2$) in neutral CS_2. This enables the nuclear wave packet to reach nonequilibrium positions in the initially bent molecule, such that only a transition from the $\tilde{X}^1A_1$ ground state to the $\tilde{B}^1B_2$ excited state becomes dipole allowed (black arrow in Fig. 3*A*) in the bent geometry (C_{2v}). Our quantum dynamical calculations confirm that symmetric stretching and bending in the laser field occurs, leading to an estimated population of about 3% in the $\tilde{B}^1B_2$ state in neutral CS_2. Our calculations for neutral CS_2 in Fig. 4*A* show that the molecule in the excited state bends up to about 120° at t = 0 fs (i.e., near the maximum of the pulse envelope; red oval in Fig. 4*A*). The wave packet in the $\tilde{B}^1B_2$ state then proceeds to find its lowest-energy equilibrium position (R_{eq} = 1.64 Å and Φ_{SCS} = 130°) (16–19), as shown in Fig. 3*B*. Other excited electronic states are not populated due to small dipole couplings, even in the deformed geometry. Since the energy gap of $\tilde{B}^1B_2$ relative to the ground state is ∼4.5 eV according to our calculations, the strong tunneling

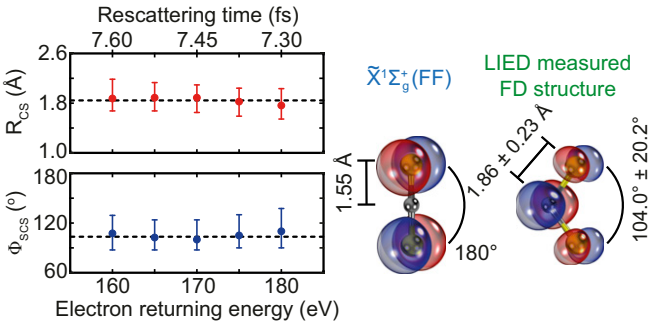

Fig. 2. Stretching and bending of field-dressed CS_2. Geometrical parameters of CS_2 are retrieved as a function of the electron returning energy. By fitting a constant line, we estimate a C-S bond length R_{CS} = 1.86 ± 0.23 Å and a S-C-S angle Φ_{SCS} = 104.0° ± 20.2°, which correspond to a strongly symmetrically stretched and bent neutral CS_2. *Top Left* shows the return time of the rescattered electrons. *Right* shows models with molecular orbitals for field-free (FF) neutral CS_2 in the ground electronic state, $\tilde{X}^1\Sigma_g^+$, and the LIED-measured field-dressed (FD) structure. The corresponding R_{CS} and Φ_{SCS} values for these two structures are indicated.

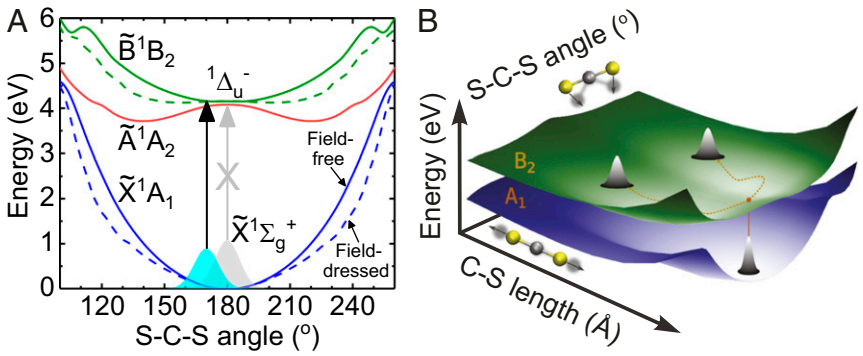

Fig. 3. Renner–Teller excitation mechanism in neutral CS_2. (*A*) Potential energy curves (PECs) for the field-free (solid curves) neutral CS_2 in the ground electronic state along with the $\tilde{X}^1A_1$ (blue), the $\tilde{A}^1A_2$ (red), and the $\tilde{B}^1B_2$ (green) excited electronic states are shown as a function of the S-C-S angle at fixed R_{CS} = 1.86 Å. The corresponding field-dressed (dashed curves) PECs are also shown. In the linear geometry ($D_{\infty h}$), a transition from the $\tilde{X}^1\Sigma_g^+$ ground electronic state to the $^1\Delta_u$ excited electronic state is dipole forbidden (gray vertical arrow) due to symmetry considerations. However, our calculations show that the molecule begins to bend by 10° (C_{2v}) in the presence of a strong field. At the same time, at bent geometries, the twofold degeneracy of $^1\Delta_u$ is lifted and splits into two distinct bent excited electronic states: $\tilde{A}^1A_2$ and $\tilde{B}^1B_2$. At these bent geometries, a transition from the $\tilde{X}^1A_1$ ground state to the $\tilde{B}^1B_2$ excited state becomes dipole allowed (black vertical arrow). (*B*) Potential energy surfaces (PESs) of field-dressed (FD) CS_2 in the $\tilde{X}^1A_1$ ground electronic state and the $\tilde{B}^1B_2$ excited state. Once the $\tilde{B}^1B_2$ state is populated, the nuclear wave packet evolves toward the equilibrium position of the $\tilde{B}^1B_2$ state.

ionization from $\tilde{B}^1B_2$ completely dominates, which permits the identification of the $\tilde{B}^1B_2$ state. Moreover, our dynamical calculations also show that the geometry of the cation (1.74 Å, 102°) does not change significantly relative to the deformed excited neutral (1.70 Å, 117°) within half a laser cycle after tunnel ionization from the $\tilde{B}^1B_2$ state (i.e., during the 7- to 8-fs excursion time of the rescattering electron; green oval in Fig. 4*B*).

The exact geometry of neutral CS_2 in the $\tilde{B}^1B_2$ excited electronic state is still discussed (19, 20); spectroscopic measurements by Jungen et al. (17) reported a quasilinear structure (1.544 ± 0.006 Å, 163°), while a much more recent analysis of the rotational progressions in the $\tilde{B}^1B_2 \leftarrow \tilde{X}^1\Sigma_g^+$ spectrum led to a largely corrected, significantly bent geometry (1.64 Å, 131.9°) (21). These measurements in fact indirectly retrieve structural information. Our directly measured structure (1.86 ± 0.23 Å, 104.0° ± 20.2°) is in general agreement with previous theoretical investigations (~1.64 Å, ~130°) (18–20) into neutral CS_2 in the $\tilde{B}^1B_2$ excited state. The MCF that corresponds to the quasilinear geometry previously measured (1.544 ± 0.006 Å, 163°) (17) does not agree with our measured data. In contrast, our results clearly support a symmetrically stretched and strongly bent molecular structure. Analogous observations of CS_2 skeletal deformation have been recently reported by Yang et al. (22), who imaged an increase in R_{CS} by 0.16 Å and 0.20 Å with respect to the equilibrium bond length when a 60-fs, 800-nm laser pulse is increased in intensity from 1.3×10^{13} Wcm^{-2} to 2.4×10^{13} Wcm^{-2}, respectively. An assumed linear extrapolation of their results would produce a 0.43-Å bond length increase for the intensity we use (9×10^{13} Wcm^{-2}), which is fully consistent with the value reported here of 0.31 ± 0.23 Å. This corresponds to strongly symmetrically stretched C-S bonds in vibronically excited neutral CS_2. Although clear indications of symmetric bond elongation were observed by Yang et al. (22), no firm conclusion was drawn about the bending vibration because of the limited spatial resolution (1.2 Å) of their ultrafast electron diffraction (UED) probe, due to the small momentum transfer of their scattered electrons (<3.5 $Å^{-1}$). It should also be noted that Yang et al. (22) used a field-free probe of molecular structure through UED with an ~400-fs pulse duration. Moreover, the lack of an electron–ion coincidence-based detection scheme added further ambiguity to the physical mechanism behind

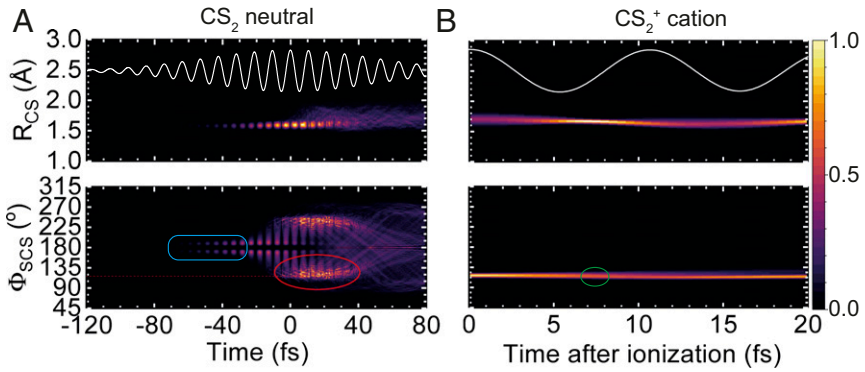

Fig. 4. Quantum dynamical wave packet calculations. (*A* and *B*) The stretching (*Top*) of C-S internuclear distance, R_{CS}, and bending (*Bottom*) of the S-C-S bond angle, ϕ_{SCS}, for (*A*) neutral CS_2 in the $\tilde{B}^1B_2$ state and (*B*) CS_2^+ cation. The starting conditions used are (*A*) neutral CS_2 in the $\tilde{X}^1\Sigma_g^+$ ground electronic state (1.55 Å, 180°) and (*B*) neutral CS_2 in the $\tilde{B}^1B_2$ excited electronic state (1.7 Å, 117°). The blue rectangle indicates the initial bending of neutral CS_2. The red (green) oval indicates the relevant structure at around the time of ionization (rescattering), t_i (t_r). Here, molecules are 90° to the laser polarization. In *A*, t = 0 fs corresponds to the peak of the 85-fs (FWHM) 3.1-μm pulse envelope, while in *B* the time axis corresponds to the time after ionization. The corresponding laser field is shown as white traces in *A* and *B*, *Top*.

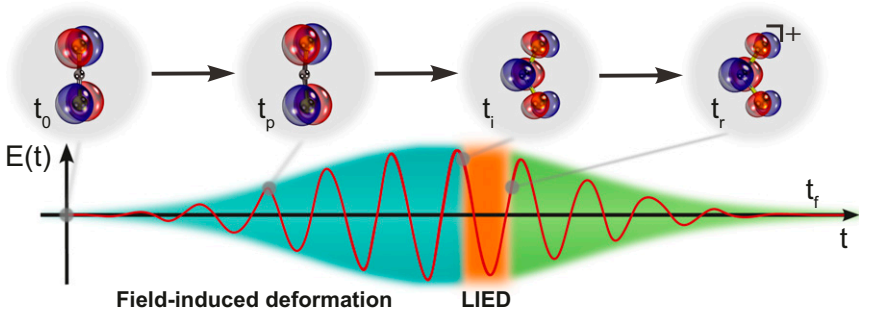

Fig. 5. Illustration of field-induced deformation and LIED measurement. In our LIED measurement, the neutral CS_2 molecule is first symmetrically stretched and initially bent by 10° (at time t_p) before leading to the significantly bent CS_2 structure at the time of ionization, t_i. A high-resolution snapshot is recorded by the high-energy electrons at the point of rescattering, t_r.

the IR-induced excitation, with two possible mechanisms suggested by the authors: excitation of an electronic state through a multiphoton process and formation of ions with longer bond lengths.

We use LIED to directly retrieve the geometric transformation of neutral CS_2 due to the Renner–Teller effect. Our measurements unambiguously identify a bent and symmetrically stretched CS_2 molecule (R_{CS} = 1.86 ± 0.23 Å, Φ_{SCS} = 104.0° ± 20.2°) that is most likely populating the $\tilde{B}^1B_2$ excited electronic state. This finding is also supported by our state-of-the-art quantum dynamical ab initio molecular dynamics calculations, which describe the linear-to-bent $\tilde{B}^1B_2 \leftarrow \tilde{X}^1\Sigma_g^+$ transition in neutral CS_2. Moreover, previous theory and indirect measurements of neutral CS_2 in the $\tilde{B}^1B_2$ excited state also broadly support our LIED measurement and calculations (18–21).

We find that the nuclear distortion in fact first proceeds through the stretching of the C-S bonds before the molecule departs from the linear geometry and begins to bend on the rising edge of the LIED pulse (at time t_p in Fig. 5). Consequently, a bent neutral CS_2 molecule most likely in the $\tilde{B}^1B_2$ excited electronic state is preferentially subsequently ionized at the peak of the pulse (at time t_i in Fig. 5) to initiate the LIED process. LIED is the elastic rescattering of the highly energetic returning EWP onto the molecular ion (at time t_r in Fig. 5), with structural information embedded within the rescattered EWP's momentum distribution at the time of recollision (*Methods*) (12, 14, 23). Here, the returning EWP scatters against the CS_2^+ molecular ion (at time t_r), which has a similar strongly stretched and bent geometry to that of the neutral CS_2 in an excited electronic state at the point of ionization (at time t_i in Fig. 5). However, during the excursion time of the returning electron of about 7–8 fs, vibrational dynamics on the cationic potential energy curves in the presence of the laser field occur. During that time, as our calculations show (green oval in Fig. 4*B*), the excited cation bends slightly farther, leading to a structure that is in good agreement with the experimentally observed bent and stretched structure.

Ultimately, our results illustrate the utility of intrapulse LIED to retrieve structural transformation with combined picometer and attosecond resolution, allowing us to directly visualize nonadiabatic dynamics in molecular systems.

Methods

Mid-IR Optical Parametric Chirped Pulse Amplifier Source. A home-built optical parametric chirped pulse amplifier (OPCPA) setup generates 85-fs, 3.1-μm pulses at a 160-kHz repetition rate with up to 21 W output power (24, 25). The OPCPA system is seeded by a passively carrier-envelope-phase (CEP) stable frequency comb generated by the difference frequency of a dual-color fiber laser system (26). The mid-IR wavelength of 3.1 μm ensures that the target is strong-field ionized in the tunneling regime. The laser pulse is focused to a spot size of 6–7 μm, resulting in a peak intensity of 9×10^{13} Wcm^{-2}.

Reaction Microscope Detection System. The experimental setup is based on a reaction microscope (ReMi) which has been previously described in detail in refs. 27–29. Briefly, a doubly skimmed supersonic jet of carbon disulfide provides the cold molecular target with a rotational temperature of <100 K. Homogeneous electric and magnetic extraction fields are employed to guide the ionic fragments and the corresponding electrons to separate detectors in the ReMi. Each detector consists of delay line detectors (Roentdek) which record the full 3D momenta of charged particles from a single molecular fragmentation event in full electron–ion coincidence. In all experiments, the laser polarization is aligned perpendicular to the spectrometer axis, parallel to the jet.

Molecular Structure Extraction. Structural information of the molecular sample is retrieved from the electron momentum distribution within the frame of the QRS theory and the independent atomic-rescattering model (IAM) (30–32). We extracted the molecular DCS from the experimental photoelectron momentum distribution as previously described in ref. 14. See *SI Appendix* for further details.

ACKNOWLEDGMENTS. We thank A. Stolow and J. Küpper for helpful and inspiring discussions. We acknowledge financial support from the Spanish Ministry of Economy and Competitiveness (MINECO), through the "Severo Ochoa" Programme for Centres of Excellence in R&D (SEV-2015-0522) Fundació Cellex Barcelona and the Centres de Recerca de Catalunya (CERCA) Programme/Generalitat de Catalunya. K.A., M.S., T.S., A.S., M.H., M.G.P., B.W., and J.B. acknowledge the European Research Council (ERC) for ERC Advanced Grant TRANSFORMER (788218), MINECO for Plan Nacional FIS2017-89536-P, Agència de Gestió d'Ajuts Universitaris i de Recerca for 2017 SGR1639, and Laserlab-Europe (EU-H2020 654148). K.A., J.B., M.L., and R. Moszynski acknowledge the Polish National Science Center within the project Symfonia, 2016/20/W/ST4/00314. A.S. and J.B. acknowledge Marie Sklodowska-Curie Grant Agreement 641272. F.J.G.d.A. acknowledges help from MINECO (MAT2017-88492-R) and the ERC (Advanced Grant 789104-eNANO). C.M. and S.G. acknowledge the ERC Consolidator Grant QUEMCHEM (772676). L.Y. and S.G. acknowledge funding from the German Research Foundation, Grant GR 4482/2. A.-T.L. and C.D.L. are supported by the US Department of Energy under Grant DE-FG02-86ER13491. M.L. acknowledges support from the Ministerio de Economía y Competitividad through Plan Nacional (Grant FIS2016-79508-P FISICATEAMO), de Catalunya (Grant SGR 1341), the CERCA Programme, the ERC (Advanced Grant OSYRIS), and the European Union's Horizon 2020 research and innovation programme FETPRO QUIC (Grant 641122).

1. Yang J, et al. (2018) Imaging CF_3I conical intersection and photodissociation dynamics with ultrafast electron diffraction. *Science* 361:64–67.
2. Attar AR, et al. (2017) Femtosecond x-ray spectroscopy of an electrocyclic ring-opening reaction. *Science* 356:54–59.
3. Worth GA, Cederbaum LS (2004) Beyond Born-Oppenheimer: Molecular dynamics through a conical intersection. *Annu Rev Phys Chem* 55:127–158.
4. Barbatti M, et al. (2010) Relaxation mechanisms of UV-photoexcited DNA and RNA nucleobases. *Proc Natl Acad Sci USA* 107:21453–21458.
5. Kleinermanns K, Nachtigallová D, de Vries MS (2013) Excited state dynamics of DNA bases. *Int Rev Phys Chem* 32:308–342.
6. Bellshaw D, et al. (2017) Ab-initio surface hopping and multiphoton ionisation study of the photodissociation dynamics of CS_2. *Chem Phys Lett* 683:383–388.

7. Wang K, McKoy V, Hockett P, Stolow A, Schuurman MS (2017) Monitoring nonadiabatic dynamics in CS_2 with time- and energy-resolved photoelectron spectra of wavepackets. *Chem Phys Lett* 683:579–585.
8. Renner R (1934) Zur Theorie der Wechselwirkung zwischen Elektronen- und Kernbewegung bei dreiatomigen, stabförmigen Molekülen [On the theory of the interaction between electronic and nuclear motion in tri-atomic rod-shaped molecules]. *Z Phys* 92:172–193. German.
9. Herzberg G (1966) Molecular spectra and molecular structure: III. *Electronic Spectra and Electronic Structure of Polyatomic Molecules* (D. Van Nostrand Company, Inc., Princeton, NJ), Vol 1.
10. Meckel M, et al. (2008) Laser-induced electron tunneling and diffraction. *Science* 320: 1478–1482.
11. Okunishi M, Niikura H, Lucchese RR, Morishita T, Ueda K (2011) Extracting electron-ion differential scattering cross sections for partially aligned molecules by laser-induced rescattering photoelectron spectroscopy. *Phys Rev Lett* 106:063001.
12. Blaga CI, et al. (2012) Imaging ultrafast molecular dynamics with laser-induced electron diffraction. *Nature* 483:194–197.
13. Xu J, et al. (2014) Diffraction using laser-driven broadband electron wave packets. *Nat Commun* 5:4635.
14. Pullen MG, et al. (2015) Imaging an aligned polyatomic molecule with laser-induced electron diffraction. *Nat Commun* 6:7262.
15. Pullen MG, et al. (2016) Influence of orbital symmetry on diffraction imaging with rescattering electron wave packets. *Nat Commun* 7:11922.
16. Wolter B, et al. (2016) Ultrafast electron diffraction imaging of bond breaking in di-ionized acetylene. *Science* 354:308–312.
17. Jungen C, Malm D, Merer A (1973) Analysis of a $^1\Delta_u$–$^1\Sigma^+_g$ transition of CS_2 in the near ultraviolet. *Can J Phys* 51:1471–1490.
18. Zhang Q, Vaccaro PH (1995) Ab initio studies of electronically excited carbon disulfide. *J Phys Chem* 99:1799–1813.
19. Wiberg KB, Wang Y-G, de Oliveira AE, Perera SA, Vaccaro PH (2005) Comparison of CIS- and EOM-CCSD-calculated adiabatic excited-state structures. Changes in charge density on going to adiabatic excited states. *J Phys Chem A* 109:466–477.
20. Brown ST, Van Huis TJ, Hoffman BC, Schaefer HF, III (1999) Excited electronic states of carbon disulphide. *Mol Phys* 96:693–704.
21. Brasen G, Leidecker M, Demtröder W, Shimamoto T, Kato H (1998) New vibrational analysis of the $^1B_2$ ($^1\Delta_u$) state of CS_2. *J Chem Phys* 109:2779–2790.
22. Yang J, Beck J, Uiterwaal CJ, Centurion M (2015) Imaging of alignment and structural changes of carbon disulfide molecules using ultrafast electron diffraction. *Nat Commun* 6:8172.
23. Zuo T, Bandrauk A, Corkum PB (1996) Laser-induced electron diffraction: A new tool for probing ultrafast molecular dynamics. *Chem Phys Lett* 259:313–320.
24. Baudisch M, Wolter B, Pullen M, Hemmer M, Biegert J (2016) High power multi-color OPCPA source with simultaneous femtosecond deep-UV to mid-IR outputs. *Opt Lett* 41:3583–3586.
25. Elu U, et al. (2017) High average power and single-cycle pulses from a mid-IR optical parametric chirped pulse amplifier. *Optica* 4:1024–1029.
26. Thai A, Hemmer M, Bates PK, Chalus O, Biegert J (2011) Sub-250-mrad, passively carrier-envelope-phase-stable mid-infrared OPCPA source at high repetition rate. *Opt Lett* 36:3918–3920.
27. Moshammer R, Unverzagt M, Schmitt W, Ullrich J, Schmidt-Böcking H (1996) A 4π recoil-ion electron momentum analyzer: A high-resolution "microscope" for the investigation of the dynamics of atomic, molecular and nuclear reactions. *Nucl Instrum Methods Phys Res Sect B* 108:425–445.
28. Dörner R, et al. (2000) Cold target recoil ion momentum spectroscopy: A 'momentum microscope' to view atomic collision dynamics. *Phys Rep* 330:95–192.
29. Ullrich J, et al. (2003) Recoil-ion and electron momentum spectroscopy: Reaction-microscope. *Rep Prog Phys* 66:1463–1545.
30. Morishita T, Le AT, Chen Z, Lin CD (2008) Accurate retrieval of structural information from laser-induced photoelectron and high-order harmonic spectra by few-cycle laser pulses. *Phys Rev Lett* 100:013903.
31. Chen Z, Le AT, Morishita T, Lin CD (2009) Quantitative rescattering theory for laser-induced high-energy plateau photoelectron spectra. *Phys Rev A* 79:033409.
32. Lin CD, Le AT, Chen Z, Morishita T, Lucchese RR (2010) Strong-field rescattering physics–Self-imaging of a molecule by its own electrons. *J Phys B At Mol Opt Phys* 43:122001.